Dependence of Singular Vector Structure and Evolution on the Choice of Norm

HYUN MEE KIM AND MICHAEL C. MORGAN

Department of Atmospheric and Oceanic Sciences, University of Wisconsin—Madison, Madison, Wisconsin

(Manuscript received 27 November 2001, in final form 22 May 2002)

ABSTRACT

A diagnosis of singular vector (SV) evolution in the Eady model for the potential enstrophy and energy norms is performed using potential vorticity (PV) inversion and Eliassen–Palm (E–P) flux diagnostics, and compared with the SV evolution for the streamfunction variance norm. The diagnostics reveal that the mechanism for SV amplification depends on the initial relative magnitudes of the interior PV and boundary temperature anomalies (BTAs). In addition, the relative magnitudes of the initial PV and BTAs are dependent on the norm chosen, the length scale of the perturbation, and the length of the optimization interval.

If the initial contribution of the PV to a given norm is larger than the contribution of the BTAs to that norm, then the SV evolution in that norm is governed by the baroclinic superposition of the interior PV followed by an amplification of the BTAs by winds attributed to the interior PV. In the other case, the mutual interaction of BTAs governs the SV evolution. The initial interior PV is most important for the energy and streamfunction variance SVs, but is less important for the potential enstrophy SVs. Excluding the longwave (i.e., wavelengths longer than the Eady instability cutoff) enstrophy norm SVs, for the shortwave SVs and for long optimization times, the importance of the initial interior PV is most apparent.

In the view of targeted observations, the sensitive regions indicated by the SV analysis can be identified with particular mechanisms for SV development. The forecast measure may be considered sensitive in some regions in the sense that the forecast measure exhibits a large response to small changes in the initial conditions in those regions. The potential enstrophy norm is identified as being dynamically sensitive at the boundaries in contrast to the energy and streamfunction variance norm in the midtroposphere. It is suggested that subjective PV diagnosis of sensitivity may be viewed as being consistent with an objective diagnosis of sensitivity using potential enstrophy norm SVs.

1. Introduction

Singular vectors (SVs) are those structures with a norm that amplifies most rapidly over a specified time period (the optimization interval) for a given basic state.[1] Because of the rapidly growing property of SVs, they have been proposed as an alternative means to describe the rapid growth of disturbances in the atmosphere–ocean system (e.g., Farrell 1989), and they have been used to construct the initial perturbations for ensemble prediction (e.g., Molteni et al. 1996) as well as detect regions of large sensitivity to small perturbations for the purposes of making adaptive or targeted observations (e.g., Palmer et al. 1998). In addition to these uses, SVs can be used to construct the eigenvectors of the forecast error covariance matrix for the end of the optimization interval (e.g., Ehrendorfer and Tribbia 1997).

Amplification of SVs is measured with respect to a predefined norm: the most commonly chosen norms have been streamfunction variance, potential enstrophy, and total energy. For the streamfunction variance and energy norms, SVs resemble synoptic-scale wave packets and are initially upshear tilted structures localized in the lower troposphere (e.g., Mukougawa and Ikeda 1994; Buizza and Palmer 1995; Hartmann et al. 1995; Hoskins et al. 2000). In contrast, the initial structure of SVs in the potential enstrophy norm is of large scale (e.g., Palmer et al. 1998). Joly (1995), in an examination of the stability of frontal cyclones, explored the initial structure and amplification rate for SVs in a uniform potential vorticity (PV) semigeostrophic model for a variety of norms including the enstrophy, total energy, and geopotential variance norms. Joly (1995) observed that very different SV structures could be identified depending on which norm was chosen. While it is evident from these examples that SV initial structure is dependent on the choice of the defining norm, it is not clear how the mechanisms governing SV development are

[1] Strictly speaking, SVs are only the initial structures that satisfy these conditions (refer to the definition in section 2a). For brevity, however, in this paper that disturbance that arises from an initial SV perturbation will be referred to as the SV at subsequent times.

Corresponding author address: Hyun Mee Kim, Department of Atmospheric and Oceanic Sciences, University of Wisconsin—Madison, 1225 W. Dayton Street, Madison, WI 53706.
E-mail: khm@mapmaker.meteor.wisc.edu

dependent on norm. The question of what the fundamental development mechanisms for SVs are is not an academic one as the resolution of this question may provide insight into such practical questions as where to target observing systems to improve specific forecasts or how better data assimilation schemes may be devised.

To better understand the fundamental mechanisms for SV development, the amplification of initially upshear tilted (and untilted) structures in general (e.g., Badger and Hoskins 2001, hereafter BH01) and SVs in particular (e.g., Morgan 2001; Morgan and Chen 2002) within simple Eady-type basic states have been studied. BH01 demonstrate that initially confined perturbations, characterized by a ''rich'' vertical structure, may experience rapid perturbation kinetic energy growth in baroclinic shear flows. The initial growth occurs by a process BH01 refer to as ''PV unshielding,'' wherein the kinetic energy of an initial perturbation, distinguished by vertically layered positive and negative PV anomalies, amplifies as the baroclinic shear unshields the PV due to differential advection. BH01 observed that the longer-term sustained growth of the perturbations is attributed to a coupling of thermal waves along the upper and lower boundaries of the Eady-type domain.

Amplification of the SV perturbation streamfunction (and kinetic energy for a single wavenumber perturbation) in the adiabatic, inviscid Eady model is accomplished by two mechanisms: baroclinic superposition of PV (''the Orr mechanism'') and amplification of the upper and lower boundary temperature anomalies (BTAs) by horizontal advection attributed to either the opposing BTAs or interior PV anomalies. Using a combination of PV inversion and Eliassen–Palm (E–P) flux diagnostics, Morgan (2001) described a three-stage sequence for SV development in the Eady model for the streamfunction variance norm. The growth of the initially upshear tilted SV begins as the baroclinic shear tilts the PV upright (leading to the PV being maximally superposed). During the next stage of development, the winds attributed to the PV increase the amplitude of the initially small BTAs. Finally, as the PV is tilted downshear, the interaction of the amplified BTAs describes the subsequent development. As noted above, the initial structures of the SVs vary with the choice of norm; as a consequence, it may be anticipated that the mechanisms for amplification vary with norm as well.

In this paper, using PV and E–P flux diagnostics, the initial SV structures and their subsequent developments are diagnosed for the potential enstrophy and energy norms and the results are compared with those for the streamfunction variance norm. While for the Eady model the contribution to the potential enstrophy norm amplification [defined in (2.9)] from growth of the interior PV is zero, the PV may still play a role in the SV development by amplifying the BTAs. If the PV does not play a role, it is possible the solution of the optimization problem would ''select'' an initial SV structure that possesses no PV, as it would be suboptimal for an SV structure to contain a component that does not amplify or contribute to amplification. In this study, we wish to examine which of the two scenarios outlined above is valid for the potential enstrophy norm. For the energy norm [defined in (2.13)], we seek that initial perturbation that maximizes both perturbation kinetic energy and perturbation available potential energy at the optimization time. We may anticipate that because the streamfunction variance norm is equivalent to the kinetic energy norm for a single wavenumber disturbance, there may be some modifications to the structure of the initial total quasigeostrophic (QG) perturbation energy norm SV to account for the maximization of the potential energy at the optimization time.

Section 2 contains a formulation of the SV problem for various norms and a brief review of the PV inversion and E–P flux diagnostics used in describing SV evolution. Singular vector evolutions for the potential enstrophy and the energy norms are presented in sections 3 and 4. The relative importance of the initial BTAs and the interior PV during SV evolution is described for the various norms and optimization times in section 5. Section 6 contains discussion and conclusions.

2. Formulation and diagnostics of SVs

The nondimensional QG PV equation for the Eady model is

$$\left(\frac{\partial}{\partial t} + \tilde{\Lambda} z \frac{\partial}{\partial x}\right)\left(\nabla^2 \psi' + \frac{1}{\tilde{S}} \frac{\partial^2 \psi'}{\partial z^2}\right) = 0, \qquad (2.1)$$

where $\tilde{\Lambda}$ and $\tilde{S}$ are nondimensional measures of shear and stratification, respectively, and ψ' is the perturbation streamfunction. The nondimensional thermodynamic equation is applied at the lower and upper boundaries ($z = 0$ and $z = 1$, respectively):

$$\left(\frac{\partial}{\partial t} + \tilde{\Lambda} z \frac{\partial}{\partial x}\right)\frac{\partial \psi'}{\partial z} - \tilde{\Lambda} \frac{\partial \psi'}{\partial x} = 0. \qquad (2.2)$$

By assuming solutions of the form $\psi'(x, y, z, t) = \hat{\psi}'(z) e^{\sigma t} e^{i(kx+ly)}$ and vertically discretizing (2.1) and (2.2) into M levels, the model equations may be written as an eigenvalue problem:

$$\mathbf{A}\hat{\psi}' = \sigma \hat{\psi}', \qquad (2.3)$$

where $\mathbf{A}$ is the $M \times M$ linearized dynamical operator. The M eigenvectors satisfying (2.3) $\hat{\psi}'_j$ describe the vertical structure of the disturbances supported on the basic state, while the corresponding eigenvalues σ_j are the growth rates of those disturbances.

If the eigenvectors of (2.3) form a complete set, the time evolution of an arbitrary initial disturbance ψ'_{arb} can be represented as a linear combination of these eigenvectors:

$$\psi'_{\text{arb}}(x, y, z_n, t) = \sum_{j=1}^{M} a_j \hat{\psi}'_j(z_n) e^{\sigma_j t} e^{i(kx+ly)} = (\mathbf{X}\mathbf{\Lambda}_t \mathbf{a})_n e^{i(kx+ly)} = (P_0^t \mathbf{X}\mathbf{a})_n e^{i(kx+ly)} = P_0^t \psi'_{\text{arb}}(x, y, z_n, 0), \quad (2.4)$$

where $\mathbf{X}$ represents a matrix of eigenvectors, $\mathbf{\Lambda}_t$ is a diagonal matrix with $e^{\sigma_j t}$ as its elements, $\mathbf{a}$ is the vector of projection coefficients a_j, and $P^t_{t=0} = \mathbf{X}\mathbf{\Lambda}_t\mathbf{X}^{-1} = e^{\mathbf{A}t}$, is the forward tangent propagator from time 0 to t.

For the calculation to follow, the model was discretized into $M = 51$ levels, with a basic state characterized by vertical shear of 3 m s^{-1} km^{-1} in a troposphere of 10-km depth, a Brunt–Väisälä frequency of 10^{-2} s^{-1}, a Coriolis parameter of 10^{-4} s^{-1}, and zero interior meridional PV gradients. The nondimensional time $t = 1$ corresponds to 9.3 h. The nondimensional wavenumber $k = 1$ corresponds to a wavelength of approximately 3142 km. The meridional wavenumber l is taken to be zero. The Eady model shortwave cutoff $k_c = 2.4$. Henceforth, we define longwave (shortwave) perturbations as those perturbations with zonal wavenumber $k < k_c$ ($k > k_c$).

a. Optimization problem

The calculation of SVs essentially involves selecting the projection coefficients subject to the constraints that the initial disturbance has unit amplitude in a specified norm and evolves to have maximum amplitude in a specified norm after some finite time $t = \tau_{\text{opt}}$. In this study, we choose the initial and final norms to be the same. We define the amplitude of the streamfunction in some norm C:

$$\|\psi'(t)\|_C^2 = \langle \psi'(t), \mathbf{C}\psi'(t)\rangle_{L_2} = \langle P_0^t \psi'(0), \mathbf{C}P_0^t\psi'(0)\rangle_{L_2} = \langle \psi'(0), P_0^{t\text{H}}\mathbf{C}P_0^t\psi'(0)\rangle_{L_2}, \quad (2.5)$$

where the inner product is denoted by $\langle\ \rangle$, $\mathbf{C}$ is the matrix operator appropriate to the C norm, and the superscript 'H' indicates the conjugate transpose. The norm without any specification will be taken to be the L_2 norm. The constrained optimization problem seeks to maximize the Rayleigh quotient λ^2 (the amplification factor),

$$\lambda^2 = \frac{\|\psi'(t)\|_C^2}{\|\psi'(0)\|_C^2} = \frac{\langle \psi'(0), P_0^{t\text{H}}\mathbf{C}P_0^t\psi'(0)\rangle}{\langle \psi'(0), \mathbf{C}\psi'(0)\rangle}, \quad (2.6)$$

at the time $t = \tau_{\text{opt}}$. It may be shown that the maximum of this ratio is realized when $\psi'(0)$ is the leading SV of the matrix operator P_0^t for the C norm, that is, $\psi'(0)$ satisfies

$$P_0^{t\text{H}}\mathbf{C}P_0^t\psi'(0) = \lambda^2\mathbf{C}\psi'(0). \quad (2.7)$$

1) STREAMFUNCTION VARIANCE NORM

The amplitude of streamfunction variance can be represented as

$$\|\psi'(t)\|^2 = \langle \psi'(t), \psi'(t)\rangle. \quad (2.8)$$

Thus for the streamfunction variance norm, $\mathbf{C}$ is the identity matrix. The streamfunction variance norm is proportional to the kinetic energy norm for a single wavenumber streamfunction perturbation. The streamfunction variance norm in this model is called the L_2 norm from now on because the statevector of the model is streamfunction.

2) POTENTIAL ENSTROPHY NORM

The potential enstrophy (square of the disturbance PV or variance of PV) is defined similarly to Hakim (2000) as

$$Q = \int_0^1 \int_0^{L_x} q'^2\, dx\, dz + \int_0^{L_x} [\theta'^2(x, z = 0) + \theta'^2(x, z = 1)]\, dx, \quad (2.9)$$

where q' is the interior perturbation PV and L_x is the wavelength in the zonal direction.

In terms of the model statevector, ψ', the potential enstrophy is

$$\|\psi'(t)\|_Q^2 = \langle q'_{\text{tot}}, q'_{\text{tot}}\rangle = \langle \mathbf{L}\psi'(t), \mathbf{L}\psi'(t)\rangle = \langle \psi'(t), \mathbf{L}^{\text{H}}\mathbf{L}\psi'(t)\rangle, \quad (2.10)$$

where the subscript Q represents the potential enstrophy norm. The $q'_{\text{tot}} = \{q', \theta'\}$ is the statevector of perturbation PV, which includes both the interior PV (q') as well as BTAs (θ'), where { } denotes the vector. The interior PV, defined for $0 < z < 1$, is given by

$$q'(x, z) = \nabla^2\psi' + \frac{1}{\tilde{S}}\frac{\partial^2\psi'}{\partial z^2}. \quad (2.11)$$

The BTAs are defined as

$$\theta'(x, z = 0, 1) = \left.\frac{\partial\psi'}{\partial z}\right|_{z=0,1}. \quad (2.12)$$

Thus for the potential enstrophy norm, $\mathbf{C} = \mathbf{L}^{\text{H}}\mathbf{L}$, where the elliptic operator $\mathbf{L}$ is defined by $\mathbf{L}\psi' = \{q', \theta'\}$.

3) TOTAL QG DISTURBANCE ENERGY NORM

The total QG disturbance energy norm is defined by

$$E = \frac{1}{2}\int_0^1 \int_0^{L_x} \left(|\mathbf{v}_g|^2 + \frac{1}{\tilde{S}}\theta'^2\right) dx\, dz = \frac{1}{2}\int_0^1 \int_0^{L_x} \left[(k^2 + l^2)\psi'^2 + \frac{1}{\tilde{S}}\left(\frac{\partial\psi'}{\partial z}\right)^2\right] dx\, dz. \quad (2.13)$$

From this we may deduce the operator $\mathbf{C} = \mathbf{E}$, the QG disturbance energy norm of streamfunction is then

$$\|\psi'(t)\|_E^2 = \langle \psi'(t), \mathbf{E}\psi'(t)\rangle. \quad (2.14)$$

b. PV inversion diagnosis

A diagnosis of SV development in the Eady model requires identifying the interactions between interior PV anomalies at a given height in the Eady domain with anomalies at other heights and with the BTAs. For this purpose, piecewise PV inversion is used and the PV is partitioned into three parts: lower BTA, interior PV, and upper BTA. Based on this partition, we may attribute the SV streamfunction into those parts attributed to the BTAs, $\psi'_\theta = \psi'_T + \psi'_B$, and those parts associated with the interior PV, ψ'_q. The streamfunction perturbation ψ'_T (ψ'_B) is that part of the streamfunction attributed to the upper (lower) BTAs. The streamfunction perturbation ψ'_q is calculated by solving $\mathbf{L}\psi'_q = \{q'_{sv}, 0\}$. The ψ'_θ is calculated by solving $\mathbf{L}\psi'_\theta = \{0, \theta'_{sv}\}$. The q'_{sv} and θ'_{sv} are calculated by (2.11) and (2.12), respectively, after having solved for the SV streamfunction (ψ'_{sv}).

Singular vector growth due to the advective amplification of the BTAs on a given boundary is diagnosed whenever the phase difference between the meridional winds attributed to either the interior PV or the BTAs along the opposing boundary is within 90°. The meridional velocities v'_q and v'_θ, attributed to the PV and BTAs may be calculated from the partitioned streamfunction as $v'_q = \partial\psi'_q/\partial x$ and $v'_\theta = \partial\psi'_\theta/\partial x$. The v'_θ can be partitioned into the meridional velocity attributed to the upper BTA [$v'_T = (\partial\psi'_T/\partial x)$] and that attributed to the lower BTA [$v'_B = (\partial\psi'_B/\partial x)$]. The both BTAs may be calculated as $\theta'_B = \partial\psi'_\theta/\partial z|_{z=0}$ and $\theta'_T = \partial\psi'_\theta/\partial z|_{z=1}$. The growth of an SV due to baroclinic PV superposition may be diagnosed whenever the magnitude of either the SV streamfunction or meridional velocity attributed to the interior PV increases (i.e., whenever $\|\psi'_q\|$ or $\|v'_q\|$ increases).

c. E–P flux diagnosis

An alternate diagnosis of the development of the Eady SVs may be afforded by an E–P flux perspective (e.g., Edmon et al. 1980). For application to the Eady model with $l = 0$, the E–P flux vector has only a vertical component. Growing disturbances in the Eady model (i.e., those disturbances with increasing perturbation energy) are characterized by an upward-directed E–P flux vector (i.e., a positive zonally averaged meridional heat flux).

The vertical partitioning of the SV E–P flux of Morgan (2001) is used to diagnose the relative importance of various development mechanisms. The vertical component of the SV E–P flux can be partitioned as

$$\begin{aligned}\overline{v'\theta'} &= \overline{(v'_q + v'_\theta)(\theta'_q + \theta'_\theta)} \\ &= \overline{v'_q\theta'_q} + \overline{v'_q\theta'_\theta} + \overline{v'_\theta\theta'_q} + \overline{v'_\theta\theta'_\theta}, \quad (2.15)\end{aligned}$$

where $\theta'_q = \partial\psi'_q/\partial z$.

The four interaction terms on the right-hand side of (2.15) are denoted as $q' - q'$, $q' - \theta'$, $\theta' - q'$, and $\theta' - \theta'$, respectively. The $q' - q'$ term may be used to diagnose the interior PV superposition mechanism. The $q' - \theta'$ term is associated with horizontal advection of BTAs by winds attributed to interior PV anomalies. The $\theta' - q'$ term is associated with the interaction between interior PV anomalies with the winds attributed to BTAs. The $\theta' - \theta'$ term can be used to diagnose the mutual interactions between the BTAs on opposing boundaries.

3. Evolution of the potential enstrophy SVs

Since the SV evolution is different for shortwave ($k < k_c$) and longwave ($k > k_c$) SVs (e.g., Mukougawa and Ikeda 1994; Morgan 2001), the SV evolution is described for different wavelengths for each norm. The wavenumbers $k = 1$ and $k = 5$ are chosen for the purpose. The time necessary for the shear flow to render the initially upshear tilted PV vertical is defined as τ_{Orr}. The intermediate case of SV development for τ_{opt} around τ_{Orr} for the L_2 norm [as described in Morgan (2001)] is discussed to clarify how τ_{Orr} changes depending on the choice of norm.

a. SV development for $k = 1 < k_c$ and $\tau_{opt} = 4.2$

The sequence of Figs. 1a, 1c, 1e, and 1g shows the streamfunction[2] at the times $t = 0$, 0.5, 1.8, and 4.2. The streamfunction is initially characterized by an absence of vertical tilt with maximum amplitude located at the boundaries (Fig. 1a). Shortly after the initial time, the streamfunction acquires and maintains a westward tilt with height. In the potential enstrophy norm, the streamfunction amplifies by a factor of 80.07 by τ_{opt} and resembles the unstable mode of the Eady model for this wavenumber. Figures 1b, 1d, 1f, and 1h show the evolution of the potential temperature (PT). The only dynamically important feature of the PT distribution is its distribution along the upper and lower boundaries. Initially the magnitude of the PT is largest along the boundaries and the PT is downshear tilted (Fig. 1b). The phase difference between the upper and lower BTAs is approximately 163°. As the SV evolves, this phase difference decreases to 20° at τ_{opt} and remains constant beyond this time (Figs. 1d, 1f, and 1h)—an additional indication that a growing normal mode structure dominates the disturbance structure shortly after the initial time. The decrease in the phase difference between the upper and lower BTAs may be readily interpreted from a PV perspective: that the phase difference between the upper and lower BTAs is nearly 180° at the initial time implies that the circulations attributed to BTAs are of the same sense. As a consequence of this configuration, the BTAs on the upper (lower) boundaries aid in the eastward (westward) propagation of the BTAs on the lower (upper) boundaries. This propagation continues

[2] All the variables in the figures are perturbations.

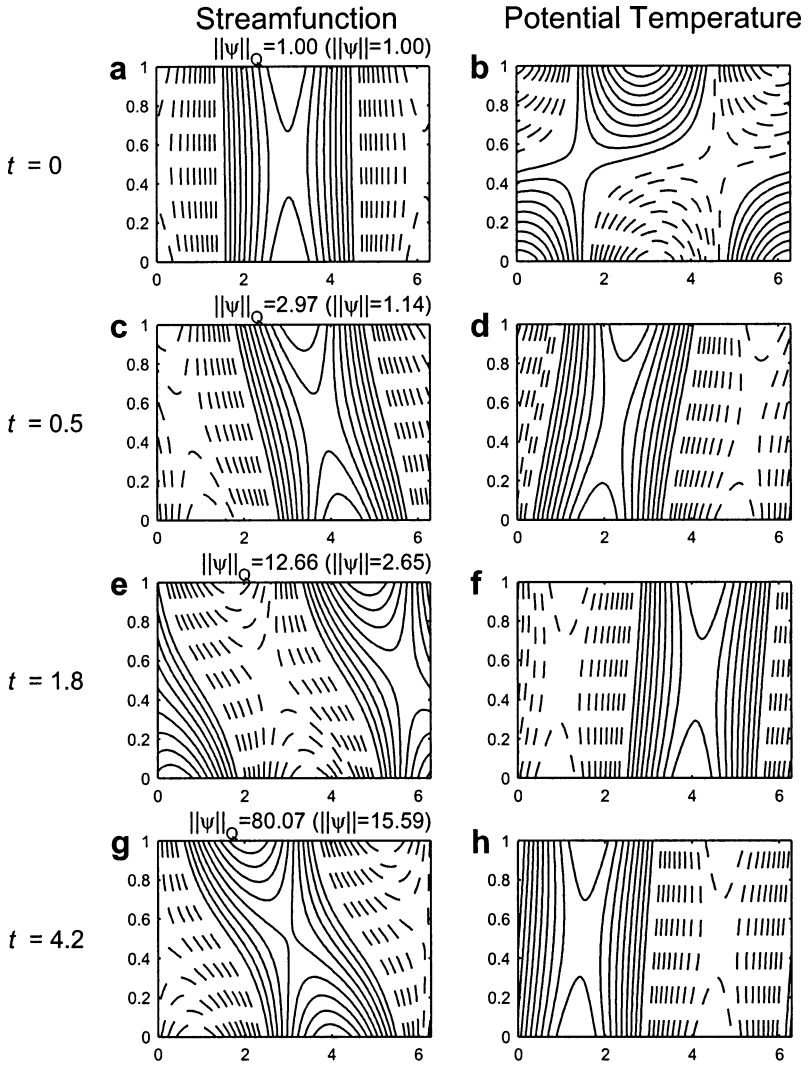

FIG. 1. Singular vector ($k = 1$, $\tau_{opt} = 4.2$) streamfunction structure for selected times for the potential enstrophy norm: (a) $t = 0$, (c) $t = 0.5$, (e) $t = 1.8$, (g) $t = 4.2$, and (b), (d), (f), (h) potential temperature structure at the same times, respectively.

until the BTAs become phase-locked (e.g., Hoskins et al. 1985).

Figure 2 shows the time evolution of the total and partitioned components of the vertical component of the E–P flux. The $q' - q'$ interaction term is approximately six to seven orders of magnitude smaller than the total term (shown in Fig. 2e). Additional experiments reveal that the amplitude of the interior PV becomes smaller as the vertical resolution of the discretization increases. This result suggests that the interior PV may be numerical noise. The $\theta' - \theta'$ term is constant with height in the interior and shows upward transport of wave activity for whole period (Fig. 2d). The meridional heat flux $\overline{v'\theta'}$ associated with the developing SVs is constant with height and is completely explained by the $\theta' - \theta'$ term (Fig. 2e).

In summary, the longwave SV evolution in the enstrophy norm is characterized by an amplification of the BTA due to the initially transient and then sustained mutual interaction of the BTAs. There is no interior PV in this SV to make a contribution to the SV amplification.

b. SV development for $k = 5 > k_c$ and $\tau_{opt} = 1.8$

Figures 3a, 3d, 3g, and 3j show the streamfunction at the selected times $t = 0$, 0.76, 1.8, and 3. In contrast to the L_2 norm, the initial streamfunction structure for the same wavenumber and optimization time resembles that of the streamfunction associated with a combination of upper and lower boundary edge waves, rather than the initially highly upstream-tilted structure seen for the $k = 5$ L_2 norm SV. In terms of potential enstrophy, the amplitude of the streamfunction is 1.08 at τ_{opt}. At $t =$

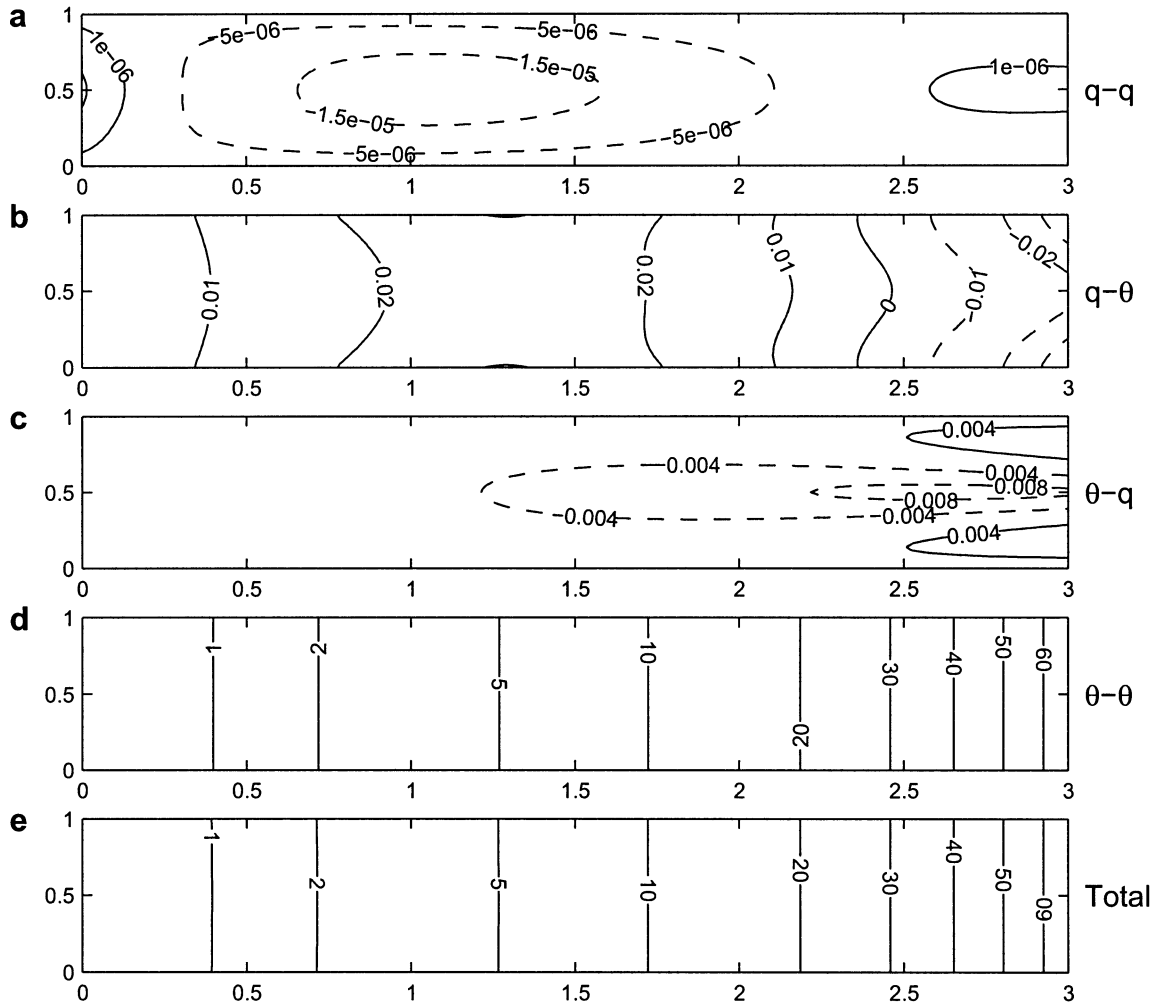

FIG. 2. Time–height cross sections of E–P flux (a) $q' - q'$, (b) $q' - \theta'$, (c) $\theta' - q'$, (d) $\theta' - \theta'$, and (e) total for $k = 1$, $\tau_{opt} = 4.2$ potential enstrophy SV.

0, the PV is tilted upshear without significant structure in the interior (Fig. 3b). The initial PV structure for this norm is maximized close to the steering level for the edge waves while for the L_2 norm the maximum amplitude is in midtroposphere. By τ_{opt}, the PV is already tilted downshear indicating that, as with the longwave SV for the potential enstrophy norm, τ_{Orr} is much shorter than the τ_{Orr} for the L_2 norm [cf. our Fig. 3h with Fig. 3h in Morgan (2001)]. The PT initially possesses no vertical tilt and has large BTAs (Fig. 3c). For all times, the PT resembles a superposition of the upper and lower edge waves (Figs. 3f, 3i, and 3l).

Because of the symmetry between the upper and lower boundaries, we focus on the development of the lower BTAs. Figure 4a shows the evolution of the magnitudes of the lower boundary meridional velocities attributed to the upper BTA (v_T'), the interior PV (v_q'), and the sum of both velocities ($v_T' + v_q'$). From Fig. 4a, it is seen that the magnitude of v_q' is larger than v_T'. The v_q' peaks at $t = 0.76$, which corresponds to the approximate time at which the PV is nearly vertical. The phase difference between v_q' and θ_B' is within $\pm 90°$ until τ_{opt} (Fig. 4b). The favorable meridional advection of lower BTA by v_T' is transient as the phase difference between the lower BTA and v_T' is continually increasing—an indication that phase locking between the upper and lower wave has not occurred.

Figure 5 displays the structure and evolution of the E–P flux. Upward-directed E–P fluxes associated with the $q' - q'$ term are maximized near the upper and lower steering levels of the neutral Eady waves until $t \sim 0.1$ (Fig. 5a), while downward-directed fluxes are maximized at time $t = 1.5$. The distribution of the E–P fluxes associated with the $q' - q'$ term are consistent with the superposition of like-signed PV anomalies as the time of maximum superposition, $\tau_{Orr} = 0.76$, occurs between the maximum upward and downward fluxes. It is noted that the superposition occurs well before τ_{opt} as seen in the longwave case. The $q' - \theta'$ term is comparable to or larger than the $\theta' - \theta'$ term (Fig. 5b). The

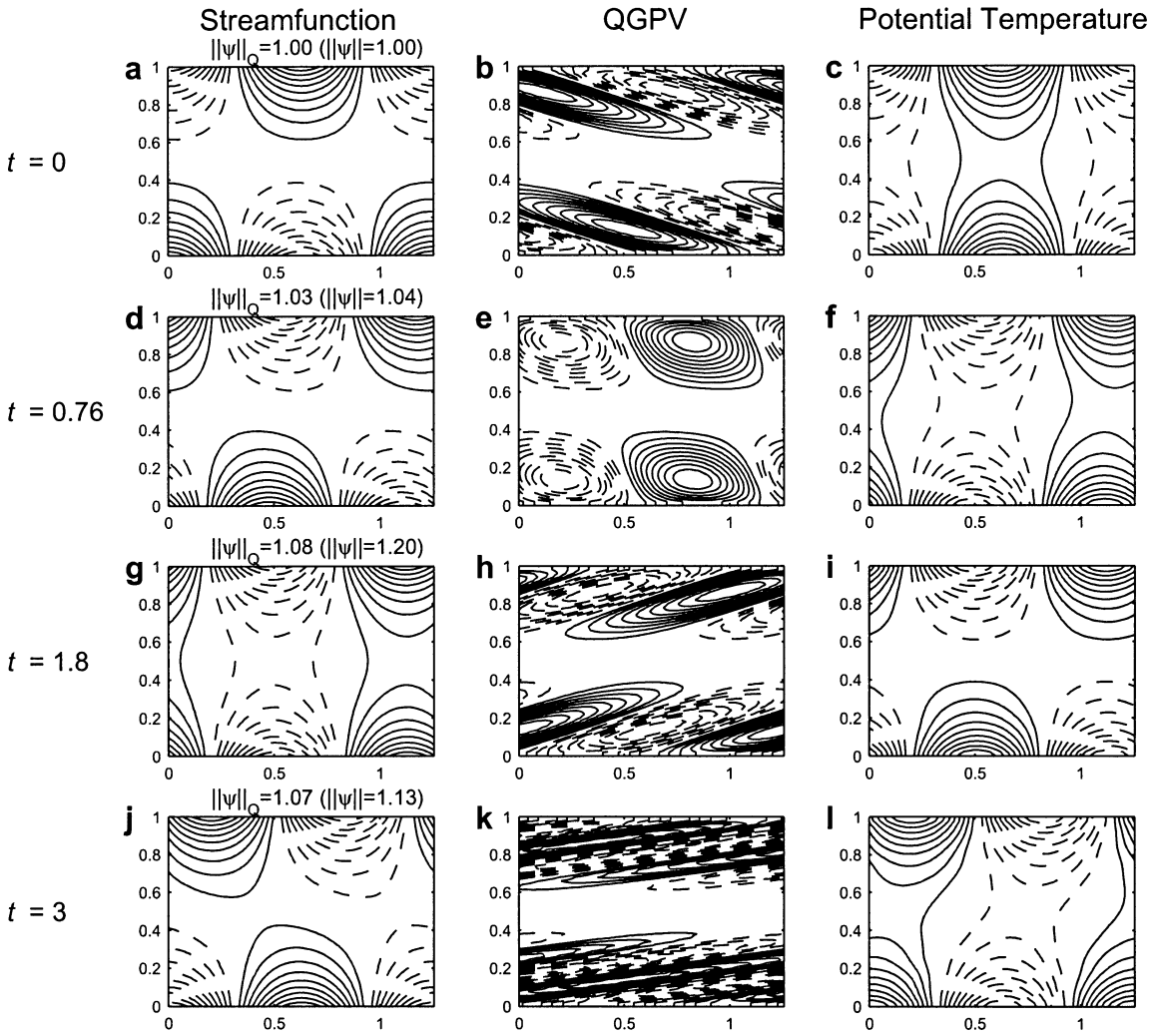

FIG. 3. Singular vector ($k = 5$, $\tau_{opt} = 1.8$) streamfunction structure for selected times for the potential enstrophy norm: (a) $t = 0$, (d) $t = 0.76$, (g) $t = 1.8$, and (j) $t = 3$; (b), (e), (h), (k) PV structure at the same times, and (c), (f), (i), (l) potential temperature structure at the same times, respectively.

meridional heat fluxes associated with the $q' - \theta'$ term are maximized near time $t = 1$ and remain positive along the boundaries until $t = 2$. Due to the transient nature of the interactions between BTAs along opposing boundaries, the $\theta' - \theta'$ term is characterized by a vertically uniform, alternating upward- and downward-directed E–P flux (positive and negative meridional heat fluxes; Fig. 5d). The total flux is also characterized by an alternating upward- and downward-directed E–P flux (Fig. 5e). Maximum values of the flux are found at the boundaries of the domain while minimum values of the flux are found in the middle of the domain. The total flux is dominated by contributions from the $q' - \theta'$ and $\theta' - \theta'$ terms.

The shortwave SV development for this optimization interval is different from that for the longwave SV and follows the three-stage SV development (Morgan 2001): initially the development is characterized by an upward flux of wave activity that is maximized in the vicinity of the steering level close to the boundaries. Next, a favorable interaction between the BTA and the PV anomalies near the steering level of the edge waves characterizes the SV growth. Finally, transient growth and decay occur as the edge waves along the opposing boundaries travel past one another.

4. Evolution of the total QG disturbance energy SVs

a. SV development for $k = 1 < k_c$ and $\tau_{opt} = 4.2$

Figures 6a, 6d, 6g, and 6j show the streamfunction at the selected times $t = 0$, 2.6, 4.2, and 6. The streamfunction is initially nearly vertical with maximum amplitude in the midtroposphere (Fig. 6a). We may infer from the streamfunction structure that the BTAs are rel-

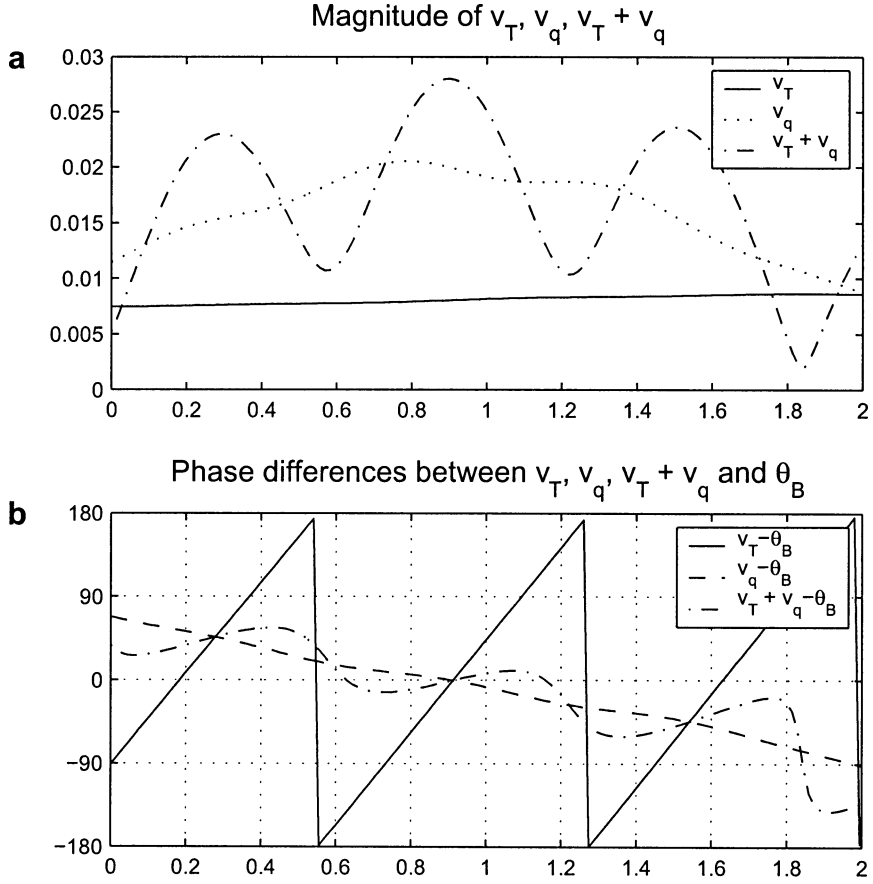

FIG. 4. For $k = 5$, $\tau_{opt} = 1.8$ potential enstrophy SV, the time evolution of the (a) magnitudes of the meridional velocities attributed to the upper boundary potential temperature anomaly (v_T'), the interior PV (v_q'), and their sum ($v_T' + v_q'$); and (b) phase differences between the meridional velocities attributed to the upper boundary potential temperature anomaly and θ_B' ($v_T' - \theta_B'$), the interior PV and θ_B' ($v_q' - \theta_B'$), and their sum and θ_B' ($v_T' + v_q' - \theta_B'$).

atively small and that the winds are stronger at the boundaries than those of the initial L_2 norm SV (cf. with Fig. 1a in Morgan 2001). After $t = 2.6$, the disturbance resembles the unstable (growing) normal mode (Fig. 6d). In terms of energy, the streamfunction amplifies by a factor of 47.25 by τ_{opt}, before which time the maximum amplitude shifts to the boundaries (Fig. 6g). Unlike the streamfunction, the PV initially leans strongly upshear and, like the streamfunction, has maximum amplitude in the midtroposphere (Fig. 6b). At $t = 2.6$, the PV is nearly vertical (Fig. 6e). By τ_{opt}, the PV is already tilted downshear (Fig. 6h). Figures 6c, 6f, 6i, and 6l show the evolution of the PT. As inferred above, at $t = 0$, the PT has small magnitude along the boundaries. As the SV evolves, the maxima in the PT anomalies shifts to the boundaries. By $t = 2.6$, the thermal structure acquires a downshear tilt indicating that a growing normal mode structure has begun to dominate the developing disturbance (Fig. 6f).

From Fig. 7a, it is seen that after $t = 0.4$, the larger of the two magnitudes of the advecting velocities is v_T'. Before that time, the magnitude of v_q' exceeds that of v_T'. Before $t = 2$ (Fig. 7b), the phase difference between v_T' and θ_B' indicate that the v_T' is not contributing to amplification of the lower BTAs. For $t > 2$, the phase difference between v_T' and θ_B' is approximately $-90°$.

Time–height cross sections of the E–P flux are shown in Fig. 8. The $q' - q'$ term reaches a maximum at approximately $t = 1.2$, then diminishes to zero by $t = 2.6$—the time of maximum superposition (Fig. 8a). The $q' - \theta'$ term is characterized by an upward-directed E–P flux for the entire period and is maximized at the lower boundary at approximately $t = 4.6$ (Fig. 8b). The $\theta' - \theta'$ term is constant with height in the interior, and upward transport of wave activity from lower to upper boundary is diagnosed for the period $t > 2$, consistent with the phase difference between θ_B' and v_T' described above (Fig. 8d). The total zonally averaged heat flux $\overline{v'\theta'}$ associated with the developing SVs is initially smaller near the upper and lower boundaries than in the interior (Fig. 8e). During the earliest stage of development ($0 < t < 2$), the $\overline{v'\theta'}$ is explained mostly by the $q' - q'$ term and $q' - \theta'$ term. For $2 < t < 4$, both the $q' - \theta'$ term and $\theta' - \theta'$ term are important and

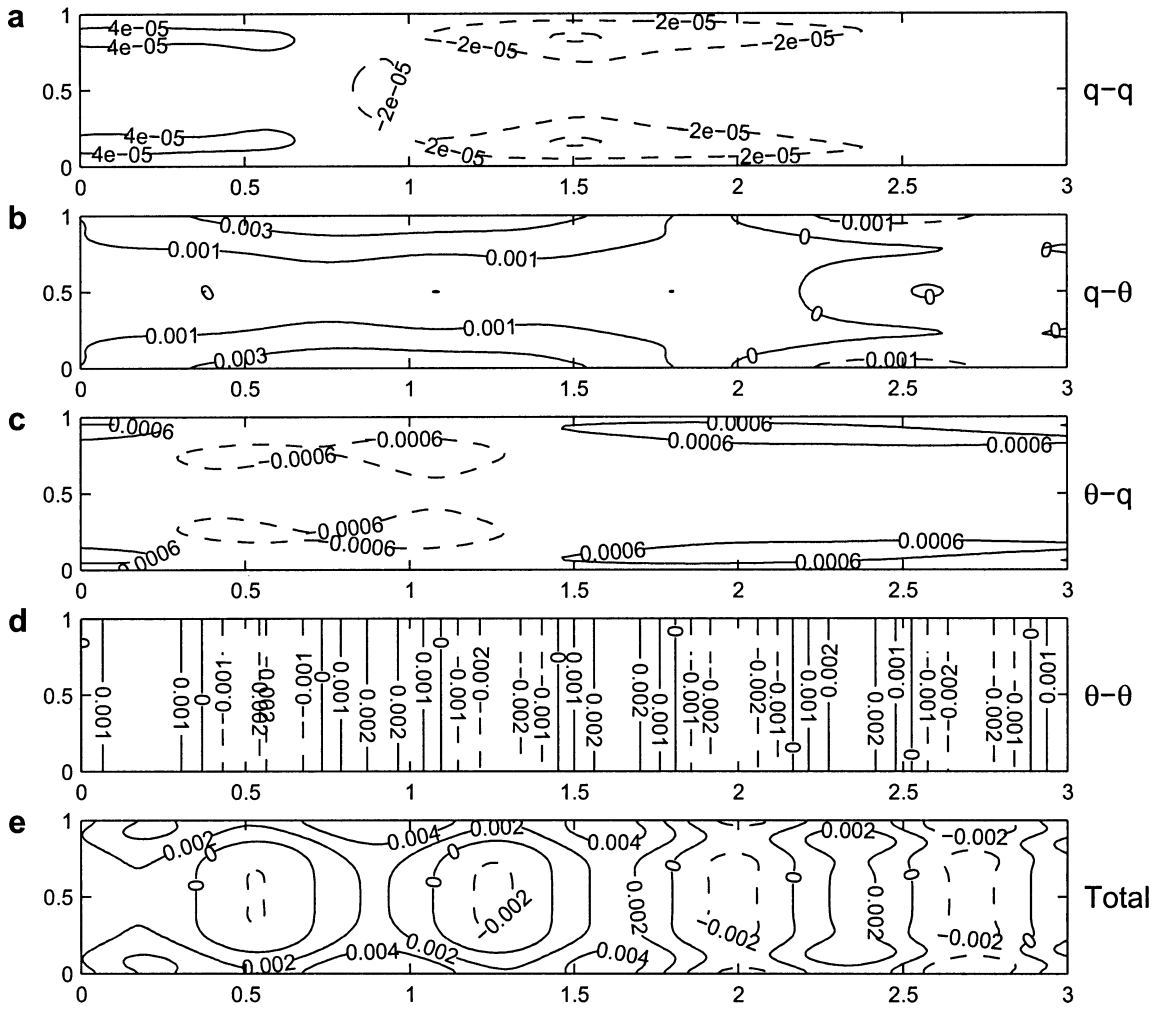

FIG. 5. As in Fig. 2, except for the $k = 5$, $\tau_{opt} = 1.8$ potential enstrophy SV.

after $t = 4$, the $\overline{v'\theta'}$ is almost exclusively described by the $\theta' - \theta'$ term.

The longwave SV evolution in the energy norm follows the three-stage SV development described for the L_2 norm; however, the baroclinic superposition of PV and amplification of BTAs occurs earlier in the evolution of the SV (compared with that of the L_2 SVs) so that after a comparatively short time, the mutual interaction of the upper and lower BTAs becomes the dominant mechanism for SV growth. In fact, for the $k = 1$, L_2 norm SV normal mode growth begin after the optimization time $\tau_{opt} = 4.2$, for this norm the normal mode growth commences at $t = 2$.

b. SV development for $k = 5 > k_c$ and $\tau_{opt} = 1.8$

Figures 9a, 9d, 9g, and 9j show the streamfunction at the selected times $t = 0$, 1.63, 1.8, and 4. The streamfunction is characterized initially by an upshear tilt with maximum amplitude in the upper and lower troposphere near the steering levels of the neutral Eady modes (Fig. 9a). In the energy norm, the streamfunction amplifies by a factor of 7.43 by τ_{opt}, and the maximum amplitude shifts to the boundaries (Fig. 9g). The PV is tilted upshear initially with maximum amplitude nearest the steering levels of the upper and lower neutral Eady modes. The PV is maximally superposed at $t = 1.63$ (Fig. 9e). The PT is also initially tilted upshear (Fig. 9c). Around τ_{opt} and time intervals beyond, the PT is maximized along the upper and lower boundaries (Figs. 9f, 9i, and 9l).

The v'_q peaks at $t = 1.6$ close to the time of maximum superposition τ_{Orr} (Fig. 10a). The phase difference between v'_q and θ'_B is favorable for BTA amplification on the time interval ($0.25 < t < 2.75$) (Fig. 10b). Amplification of the BTAs due to advections attributed to the interior PV is therefore maximized just prior to the time of τ_{Orr}.

Figure 11 displays the structure and evolution of the E–P flux. The magnitude of the $q' - q'$ term is initially maximized near both the steering levels for the neutral modes, but reaches a maximum in the midtroposphere

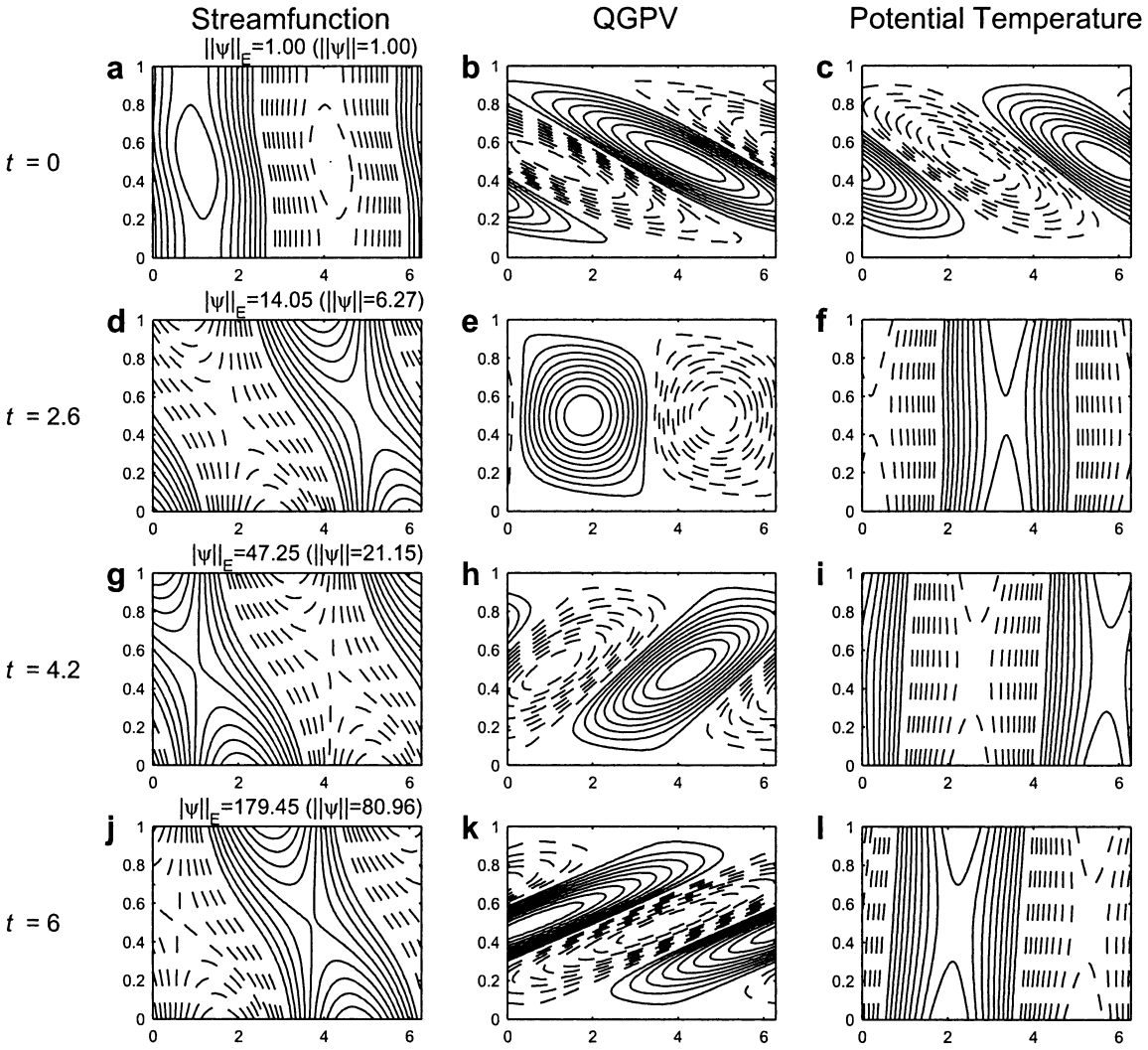

FIG. 6. As in Fig. 3, except for the $k = 1$, $\tau_{opt} = 4.2$ energy SV and $t = 0$, 2.6, 4.2, and 6.

prior to $t = 1.63$ (Fig. 11a). Downward-directed E–P fluxes are maximized at time $t = 1.9$. As was seen in the longwave case, this antisymmetric distribution of the wave activity fluxes associated with the $q' - q'$ term is consistent with the superposition and subsequent disjunction of like-signed PV anomalies. The $q' - \theta'$ term is large compared with the $q' - q'$ term and explains most of the total E–P flux distribution (cf. Fig. 11b with 11e). The $q' - \theta'$ fluxes are maximized at $t = 1.8$ and remain positive in most of the domain until $t = 2.8$. The period of positive $q' - \theta'$ fluxes corresponds to that period within which the phase difference between v'_q and θ'_B is within $\pm 90°$ in Fig. 10b. The $\theta' - \theta'$ term is characterized by a vertically uniform, alternating upward- and downward-directed E–P flux (Fig. 11d). The total E–P flux increases over the time interval $0 < t < 1.8$ in the upper and lower troposphere (Fig. 11e). Maximum values of the flux are found at the upper and lower boundaries at τ_{opt}. For $t > 1.8$, the flux is characterized by convergence (divergence) at the steering levels of the lower (upper) neutral Eady mode. The distribution of E–P flux divergence implies an increase in wave activity at both steering levels.

In summary, the PV diagnosis and the E–P flux diagnosis indicate that the shortwave SV evolution in energy norm follows the three-stage SV development very well.

5. Relative importance of the initial BTAs and interior PV

The relative importance of the initial BTAs and interior PV to the SVs' evolution in various norms can be demonstrated by eliminating either the BTAs or the PV in the initial SV structure, and allowing the modified structure to develop. Because the longwave potential enstrophy SV has no interior PV, it is not discussed in this section.

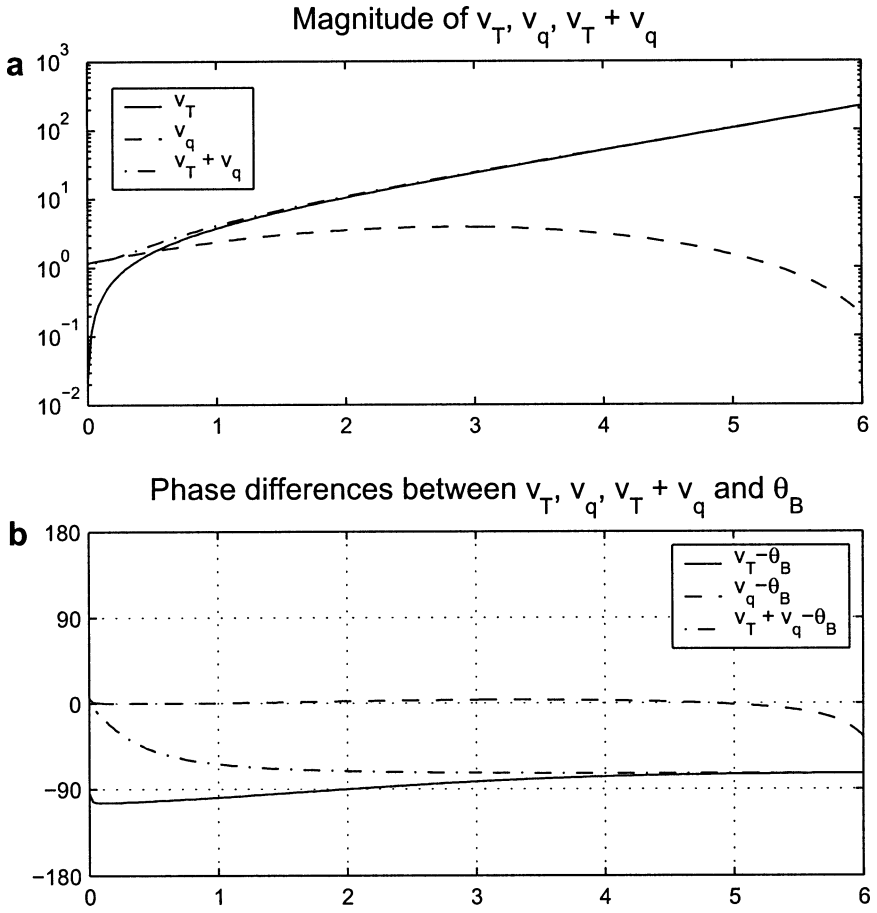

FIG. 7. As in Fig. 4, except for the $k = 1$, $\tau_{opt} = 4.2$ energy SV.

The potential enstrophy norms of the shortwave SV streamfunction, the perturbation with only initial PV ($\psi'_{q_{only}}$), and the perturbation with only initial BTAs ($\psi'_{\theta_{only}}$) are shown in Figs. 12a, 12b, and 12c for optimization times of 0.5, 1.8, and 4.2, respectively. For the shortwave SVs, the $\psi'_{\theta_{only}}$ perturbation is larger than the $\psi'_{q_{only}}$ perturbation for short optimization times (e.g., $\tau_{opt} < 0.5$), but becomes smaller than the $\psi'_{q_{only}}$ perturbation as the optimization time increases (Figs. 12b, c). In terms of the potential enstrophy norm, the $\psi'_{\theta_{only}}$ streamfunction perturbation amplifies only transiently due to transient mutual interactions of the BTAs on opposing boundaries. The potential enstrophy norm of $\psi'_{q_{only}}$ amplifies slightly as the interior PV aids in the amplification of the BTAs. It should be noted, however, that the BTAs are still necessary as the amplification of $\psi'_{q_{only}}$ alone is insufficient to explain the total SV amplification.

The energy norms of the SV streamfunction, the perturbation with only initial PV ($\psi'_{q_{only}}$), and the perturbation with only initial BTAs ($\psi'_{\theta_{only}}$) are shown in Figs. 12d–i. For the longwave SVs, for $\tau_{opt} = 0.5$ and 1.8, the initial amplitudes of the $\psi'_{q_{only}}$ disturbance are larger than the amplitude of SVs—indicating that $\psi'_{q_{only}}$ and $\psi'_{\theta_{only}}$ are nearly 180° out of phase initially and throughout the SV evolution (Figs. 12d, e). This is analogous to the PV ''masking'' described by Morgan and Chen (2002). As the optimization time increases, the $\psi'_{q_{only}}$ describes an increasing fraction of the entire evolution (Fig. 12f). The shortwave SVs show the masking for $\tau_{opt} = 0.5$ (Fig. 12g) and the $\psi'_{q_{only}}$ describes all of the entire evolution as the optimization times become longer (Fig. 12h, i).

A similar experiment for the L_2 norm is shown in Morgan (2001). The results for the shortwave SVs in L_2 norm are very similar to those for the energy norm. The longwave SVs in L_2 norm shows $\psi'_{q_{only}}$ and $\psi'_{\theta_{only}}$ are out of phase for $\tau_{opt} = 0.5$, 1.8, and 4.2, even though the $\psi'_{q_{only}}$ disturbance becomes more dominant for optimization times close to τ_{Orr}.

Figure 13 shows the relationship between τ_{opt} and the magnitude of the initial BTAs and interior PV. For the shortwave SVs in potential enstrophy norm the magnitude of the initial BTAs is larger than that of the initial interior PV for very short τ_{opt}. For $\tau_{opt} > 1.5$, the initial interior PV is larger than the initial BTAs and increases with respect to τ_{opt}. For the energy and L_2 norms, the magnitudes of the initial interior PV increase as a function of τ_{opt} for the small and intermediate optimization times

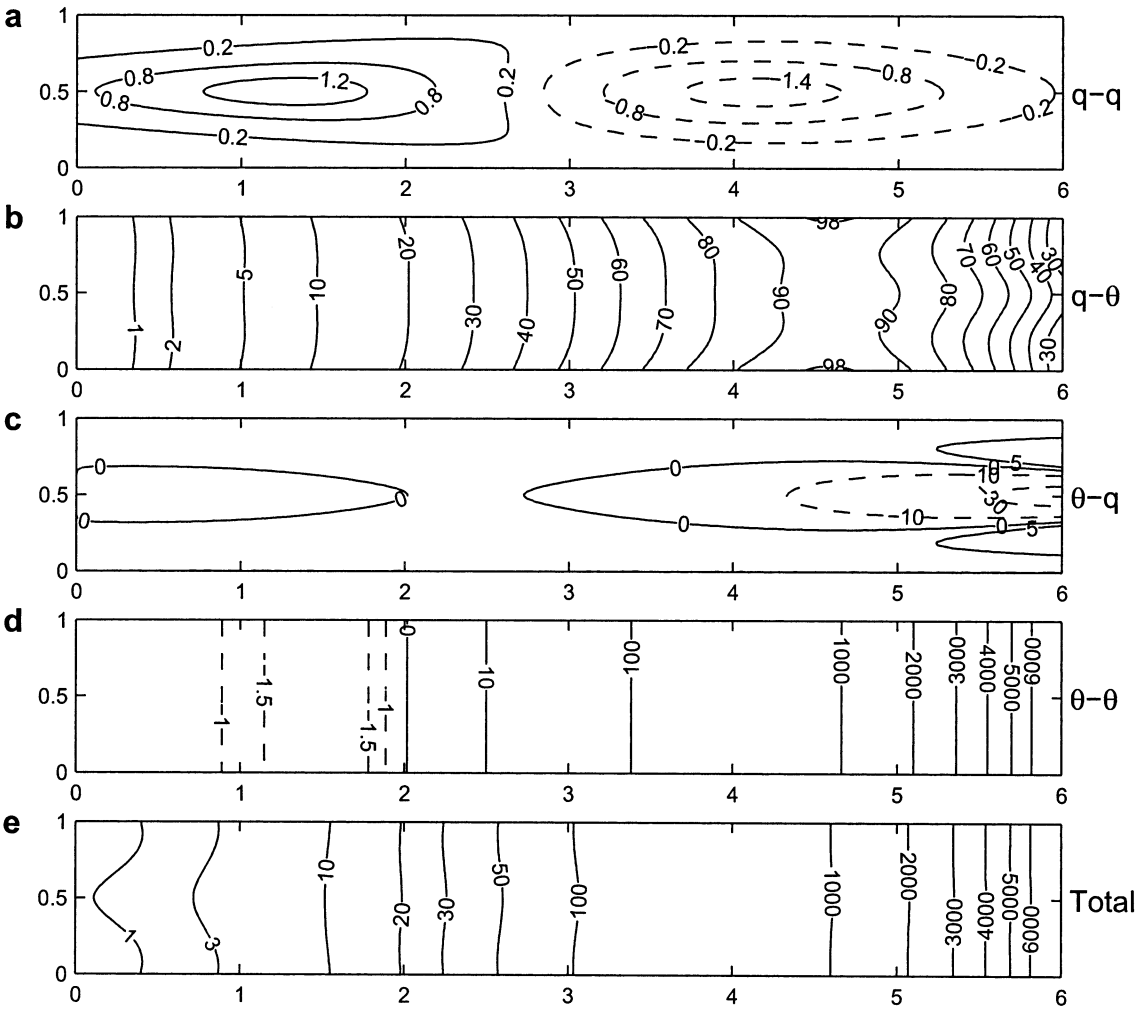

FIG. 8. As in Fig. 2, except for the $k = 1$, $\tau_{opt} = 4.2$ energy SV.

(i.e., dimensionally from several hours to a few days) and the initial interior PV is dominant for any τ_{opt}.

6. Discussion and conclusions

a. Mechanisms for growth

In this paper, the initial structures and subsequent evolution of Eady model SVs for the potential enstrophy and energy norms have been diagnosed and the results compared with those for the L_2 norm. Based on the results of piecewise PV inversions and a partitioning of the E–P fluxes associated with the SVs, it has been demonstrated that the initial structure of SVs is dependent on the choice of norm, wavenumber, and optimization interval. In addition, a relationship between the SV initial structure and the mechanisms for growth has been described: For those SVs for which the initial interior PV is important, the relevance of the three-stage SV development scenario described by Morgan (2001) is affirmed. The relative importance of the initial PV and BTAs to the SVs evolution in the potential enstrophy, energy and L_2 norms are summarized in Table 1. Ordered by the norms studied (proceeding from left to right in Table 1), for those SVs that contain PV, the initial interior PV is of increasing importance for the potential enstrophy, total perturbation energy, and L_2 norms, respectively. Excluding short optimization times for the potential enstrophy norm, the importance of initial interior PV is greater for short wavelength SVs compared with long wavelength SVs. For increasing optimization time (proceeding from top to bottom in Table 1), the importance of the initial interior PV increases as a function of optimization time for synoptically relevant optimization time intervals ($0.5 < \tau_{opt} < 5$), for those SV structures that contain PV. Below we briefly summarize and interpret the results separately for each norm studied.

For the potential enstrophy norm, the initial SV structure and the subsequent mechanisms for amplification are wavenumber dependent. Of the two amplification scenarios suggested in the introduction, the scenario in

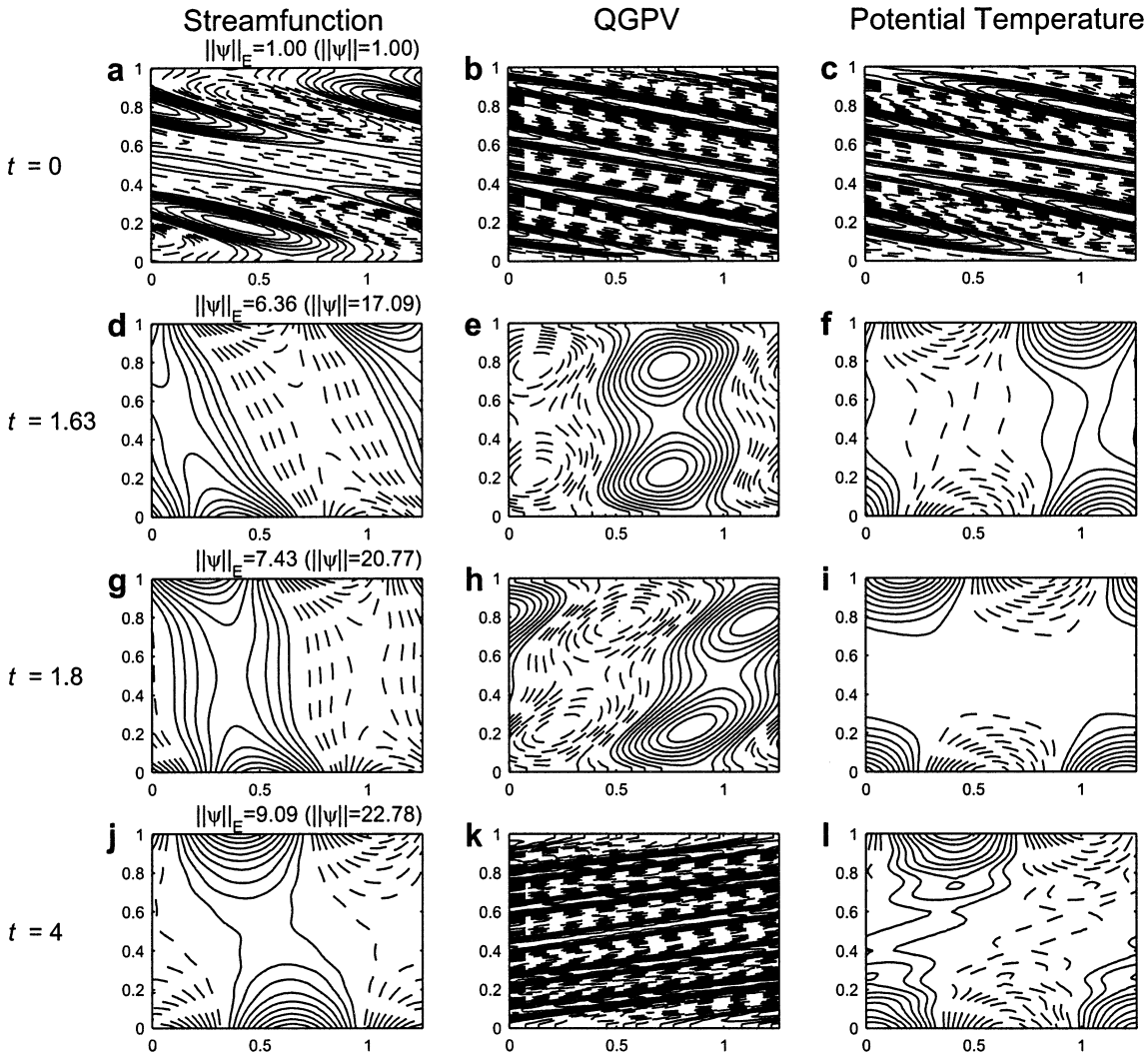

FIG. 9. As in Fig. 3, except for the $k = 5$, $\tau_{opt} = 1.8$ energy SV and $t = 0$, 1.63, 1.8, and 4.

which the solution of the optimization problem ''selects'' an initial structure with no PV is valid for longwave potential enstrophy norm SVs. For these longwave SVs, the initial SV structure consists of thermal perturbations on opposing boundaries that are nearly 180° out of phase. The thermal anomalies on one boundary enhance the edge wave propagation on the opposing boundary so that the edge modes may relatively quickly become phase locked. The resulting configuration then allows for normal mode growth to commence.

In contrast with the longwave SVs, for shortwave potential enstrophy norm SVs' interior PV does play a role in amplification. This PV, initially upshear tilted, is concentrated about the steering levels of the neutral Eady models. While the evolution of the interior PV and BTAs for this norm follows the three-stage evolution described for the L_2 norm by Morgan (2001), amplification of the BTAs by the interior PV is the dominant mechanism for development. The necessity of interior PV for the shortwave SVs for the potential enstrophy norm is simply explained: At wavenumbers beyond the Eady model shortwave cutoff, the BTAs cannot interact to produce a sustained amplification of potential enstrophy (boundary PT variance) for the optimization times longer than the interaction time (time for which the upper wave passes the lower) $t = 1.5$; consequently, SVs at these wavenumbers must be composed of both BTAs and PV. For very short optimization times, the transient interaction between the BTAs is a more efficient mechanism for development than either the interior PV superposing or the interior PV amplifying the BTAs. As the optimization time lengthens, the PV becomes increasingly concentrated at the steering level of the neutral modes and increasingly upshear tilted. This allows for a longer near-resonant interaction (with associated near-linear amplification of the BTAs) between the BTAs and the interior PV.

For the total energy norm, the initial SV structure is

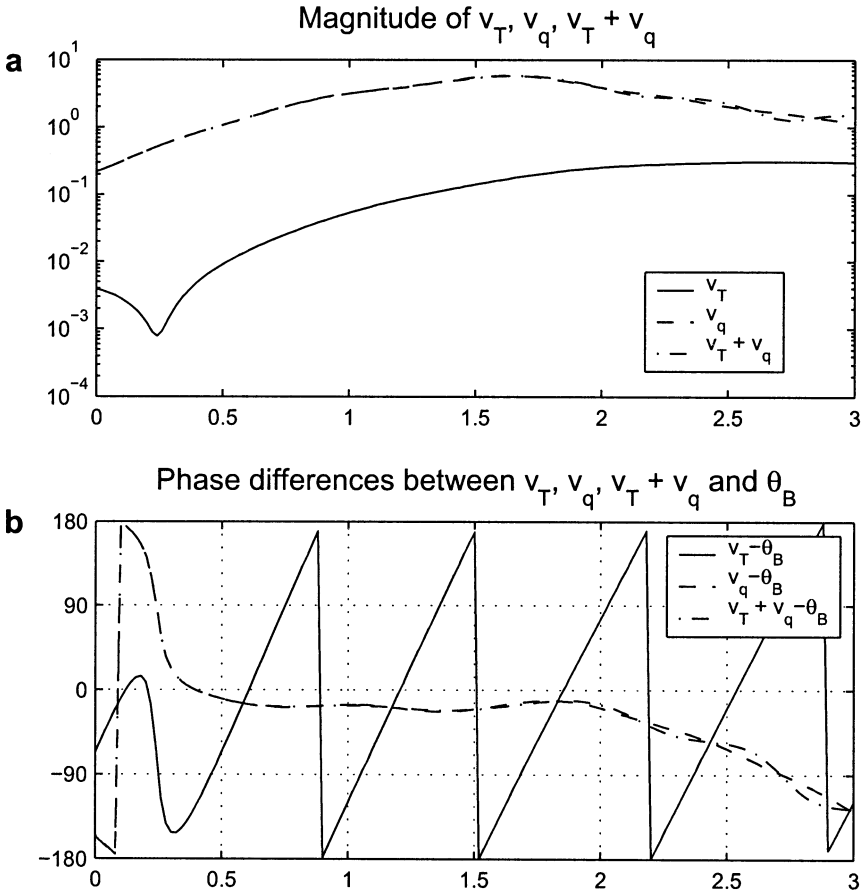

FIG. 10. As in Fig. 4, except for the $k = 5$, $\tau_{opt} = 1.8$ energy SV.

dependent on wavenumber while the growth mechanisms are not. As with the L_2 norm, the importance of the initial interior PV relative to the BTAs increases with increasing optimization time. The initial structure of SVs in this norm for all wavenumbers differs from that of the L_2 norm in that the perturbation wind at the boundaries is not negligible. As a consequence, initial development of SVs in the total energy norm is associated with both an amplification of the BTAs and a baroclinic superposition of interior PV. Following the time of maximum superposition τ_{Orr} as with the L_2 norm, the SV structure and evolution are largely governed by the mutual interactions between upper and lower BTAs for the longwave SVs, and the interactions between PV nearest the steering level of the neutral Eady modes and the BTAs for the the shortwave SVs.

As suggested in the introduction, because the L_2 norm is equivalent to the kinetic energy norm for a single wavenumber disturbance, modifications of the L_2 norm initial structure are necessary to account for the maximization of the sum of the kinetic and potential energies at the optimization time. That the PV for the total energy norm is initially less tilted than the PV of the L_2 norm (and as a consequence already tilted downshear for optimization times larger than τ_{Orr}) is consistent with the fact that for a plane wave PV disturbance, the potential energy is maximized just prior to and just following τ_{Orr} (refer to BH01's Fig. 4e). This configuration allows for the simultaneous maximizing of both the perturbation kinetic energy and potential energy in the interior due to both the interior PV and the amplified BTAs.

b. *Implication of results for targeted or adaptive observation*

As noted in the introduction, in the context of adaptive or targeted observing, SVs have been used to identify those regions in space for which additional observations, if properly assimilated, may improve a subsequent forecast. These regions may be considered sensitive in that changes to the initial conditions of a numerical weather prediction model (i.e., the analysis increments) that have a projection onto the initial SV structures in these regions will have a particularly large effect on a forecast as opposed to changes made elsewhere. Palmer et al. (1998) note that the sensitive regions identified subjectively using PV may disagree with those identified by objective SV techniques. In particular subjective (PV) diagnosis typically indicates that the regions of maximum sensitivity are in the vi-

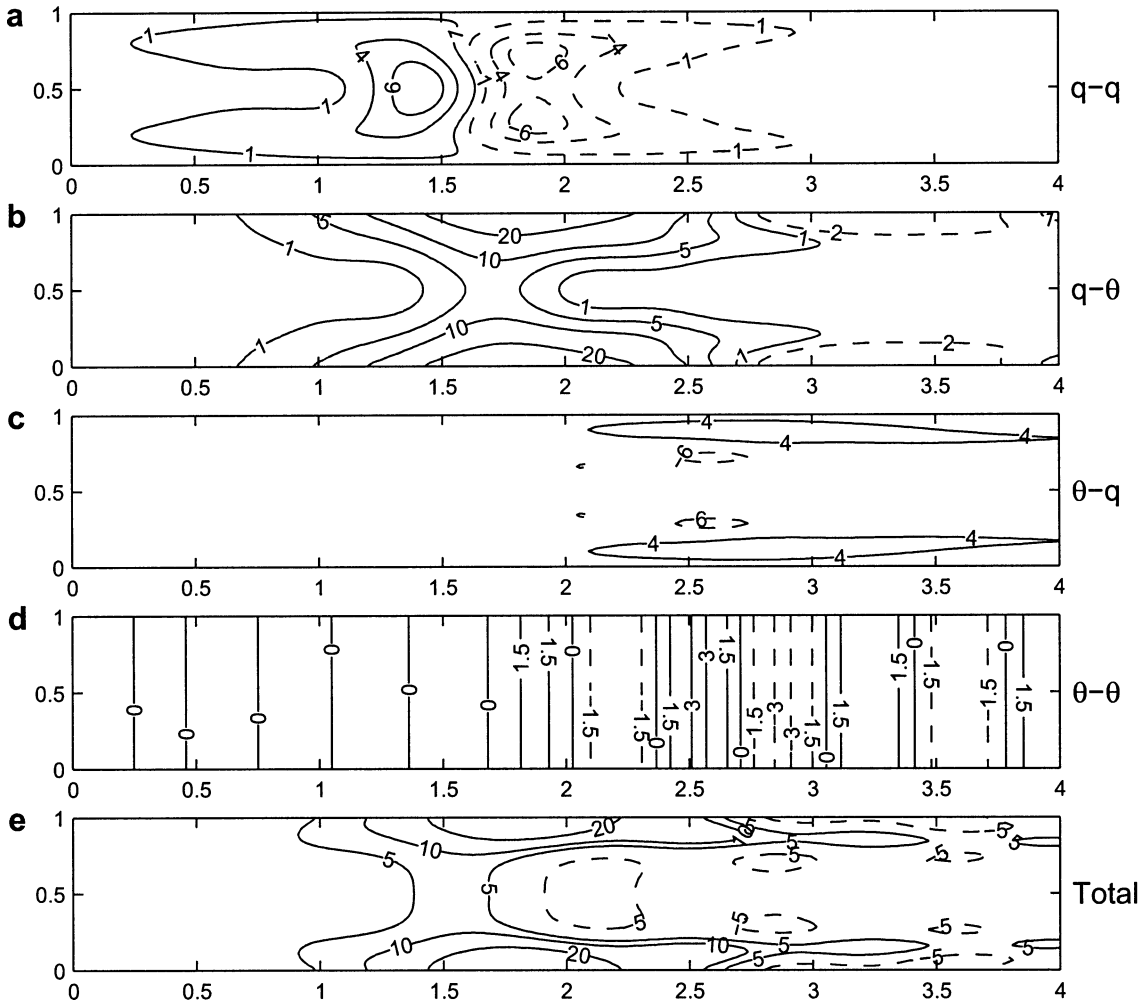

FIG. 11. As in Fig. 2, except for the $k = 5$, $\tau_{opt} = 1.8$ energy SV.

cinity of the large quasi-horizontal PT gradients along the dynamic tropopause and near the earth's surface. SV calculations, on the other hand, indicate that the lower and midtroposphere are most sensitive dynamically.

Palmer et al. (1998) argue that these differences in the identification of sensitive regions come from that fact that subjective PV diagnosis emphasizes lateral advection of PV (or advection of PT along the dynamic tropopause), while objective SV diagnosis emphasizes transport of wave activity from regions of small PV gradient (i.e., the troposphere) to regions of large PV gradient (i.e., the tropopause). Provided that wave activity is conserved, the potential enstrophy associated with an initially weak perturbation will increase if the perturbation wave activity is transfered from the lower to midtroposphere to the tropopause.

Morgan (2001) demonstrated that, for the L_2 norm SVs, amplification was in fact associated with the transport of wave activity from the lower troposphere to the tropopause as initially upshear-tilted PV structures were baroclinically superposed. The current study demonstrates that SV amplification for the total perturbation

TABLE 1. Relative importance of the initial PV and BTAs to the SVs evolution in the potential enstrophy, energy, and L_2 norms.

Norm	Potential enstrophy		Energy		L_2	
Wavenumber	$k = 1$	$k = 5$	$k = 1$	$k = 5$	$k = 1$	$k = 5$
$\tau_{opt} = 0.5$	BTAs ~ total	BTAs > PV	PV > BTAs	PV > BTAs	PV > BTAs	PV > BTAs
$\tau_{opt} = 1.8$	BTAs ~ total	BTAs > PV	PV > BTAs	PV ~ total	PV > BTAs	PV ~ total
$\tau_{opt} = 4.2$	BTAs ~ total	PV > BTAs	PV ~ total	PV ~ total	PV > BTAs	PV ~ total
$\tau_{opt} = 8$	BTAs ~ total	PV > BTAs	PV ~ total	PV ~ total	PV > BTAs	PV ~ total

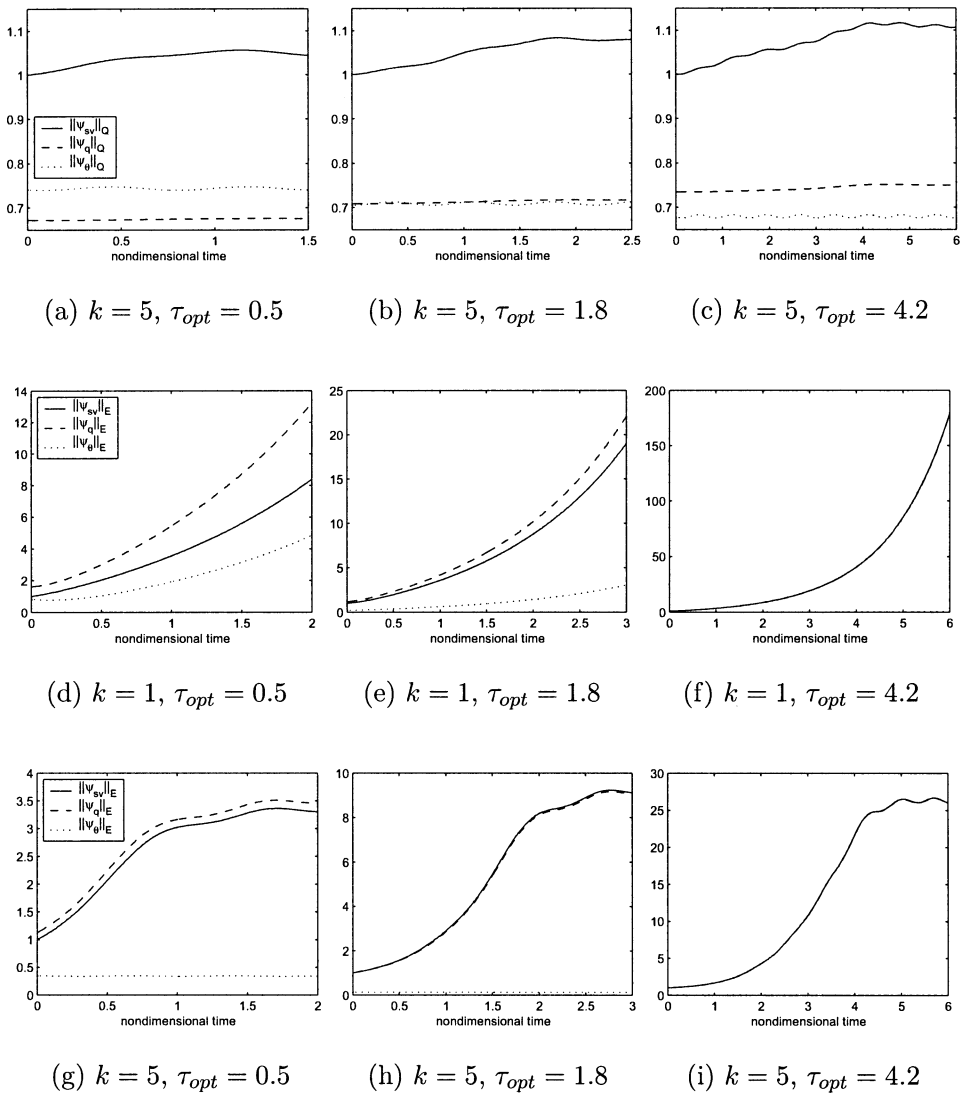

FIG. 12. The time evolution of the potential enstrophy norm of singular vector streamfunction ($\|\psi'_{sv}\|_Q$), $\psi'_{q_{only}}$ ($\|\psi'_{q_{only}}\|_Q$), and $\psi'_{\theta_{only}}$ ($\|\psi'_{\theta_{only}}\|_Q$) for $k = 5$: (a) $\tau_{opt} = 0.5$, (b) $\tau_{opt} = 1.8$, and (c) $\tau_{opt} = 4.2$. The time evolution of the energy norm of singular vector streamfunction ($\|\psi'_{sv}\|_E$), $\psi'_{q_{only}}$ ($\|\psi'_{q_{only}}\|_E$), and $\psi'_{\theta_{only}}$ ($\|\psi'_{\theta_{only}}\|_E$) for $k = 1$: (d) $\tau_{opt} = 0.5$, (e) $\tau_{opt} = 1.8$, and (f) $\tau_{opt} = 4.2$. (g), (h), (i) The same as (d), (e), and (f) except for $k = 5$.

energy and for the shortwave potential enstrophy norm SVs is also associated initially with the superposition of interior PV and concomitant upward transport of wave activity, though for the longwave total energy norm, the upward transport of wave activity from the lower boundary to the upper boundary, associated with mutual amplification of BTAs, also contributes to SV amplification. For the longwave potential enstrophy norm, this study suggests a means of reconciling the apparent discrepancy between subjective (PV) sensitivity diagnosis and objective (SV) sensitivity diagnosis. In the midlatitude troposphere, horizontal gradients of PV along isentropic surfaces are relatively small—much like the vanishing horizontal gradients of PV in the Eady model. As a consequence, subjective diagnoses of sensitive regions are equivalent to objective potential enstrophy SV diagnoses (for longwave SVs) as both approaches identify those regions of the flow for which horizontal advective amplification of PV waves is possible. Despite the lack of interior PV for this norm, SV amplification for this norm also indicates an upward transport of wave activity from the lower troposphere (the surface) to the upper troposphere (the tropopause).

If the potential enstrophy norm were chosen for the purposes of targeted observations, despite the presence of tropospheric SV streamfunction perturbation (and the implied thermal and wind perturbations) structure, only the tropopause and surface PT need be sampled (to the

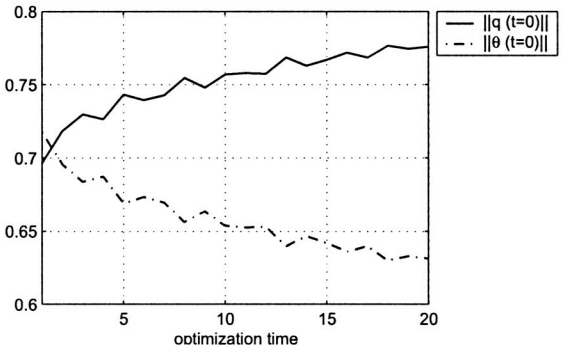

(a) $k = 5$, potential enstrophy norm

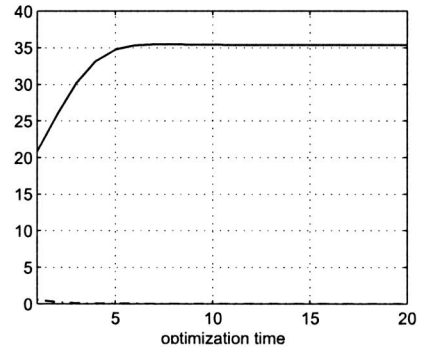

(b) $k = 1$, energy norm

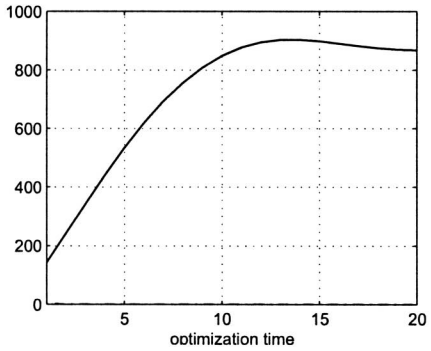

(c) $k = 5$, energy norm

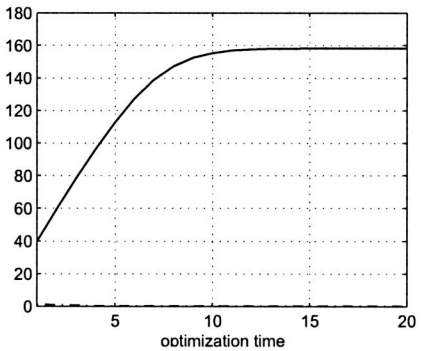

(d) $k = 1$, L_2 norm

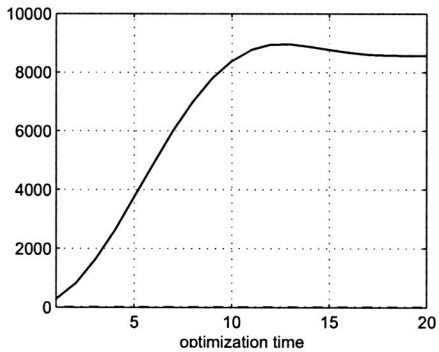

(e) $k = 5$, L_2 norm

FIG. 13. The amplitude of the initial BTAs and interior PV with respect to the optimization times.

extent that lateral gradients of PV are small). Any sampling strategy that focused on enhanced tropospheric observations or any data assimilation scheme that only created analysis increments in the troposphere based on those targeted observations, would be ineffective in reducing a subsequent forecast error in the sense of potential enstrophy norm.

Acknowledgments. The authors wish to thank Dr. Chris Snyder of the National Center for Atmospheric Research for helpful comments regarding this work. We have benefited from valuable comments provided by three anonymous reviewers. This work was supported by the National Science Foundation Grant ATM-9810916.

REFERENCES

Badger, J., and B. J. Hoskins, 2001: Simple initial value problems and mechanisms for baroclinic growth. *J. Atmos. Sci.,* **58,** 38–49.

Buizza, R., and T. Palmer, 1995: The singular vector structure of the atmospheric global circulation. *J. Atmos. Sci.,* **52,** 1434–1456.

Edmon, H. J., Jr., B. J. Hoskins, and M. E. McIntyre, 1980: Eliassen–Palm cross sections for the troposphere. *J. Atmos. Sci.,* **37,** 2600–2616.

Ehrendorfer, M., and J. J. Tribbia, 1997: Optimal prediction of forecast error covariances through singular vectors. *J. Atmos. Sci.,* **54,** 286–313.

Farrell, B., 1989: Optimal excitation of baroclinic waves. *J. Atmos. Sci.,* **46,** 1193–1206.

Hakim, G. J., 2000: Role of nonmodal growth and nonlinearity in cyclogenesis initial-value problems. *J. Atmos. Sci.,* **57,** 2951–2967.

Hartmann, D. L., R. Buizza, and T. N. Palmer, 1995: Singular vectors: The effect of spatial scale on linear growth of disturbances. *J. Atmos. Sci.,* **52,** 3885–3894.

Hoskins, B. J., M. E. McIntyre, and A. W. Robertson, 1985: On the use and significance of isentropic potential vorticity maps. *Quart. J. Roy. Meteor. Soc.,* **111,** 877–946.

——, R. Buizza, and J. Badger, 2000: The nature of singular vector growth and structure. *Quart. J. Roy. Meteor. Soc.,* **126,** 1565–1580.

Joly, A., 1995: The stability of steady fronts and the adjoint method: Nonmodal frontal waves. *J. Atmos. Sci.,* **52,** 3082–3108.

Molteni, F., R. Buizza, T. N. Palmer, and T. Petroliagis, 1996: The ECMWF ensemble prediction system: Methodology and validation. *Quart. J. Roy. Meteor. Soc.,* **122,** 73–119.

Morgan, M., 2001: A potential vorticity and wave activity diagnosis of optimal perturbation evolution. *J. Atmos. Sci.,* **58,** 2518–2544.

——, and C.-C. Chen, 2002: Diagnosis of optimal perturbation evolution in the Eady model. *J. Atmos. Sci.,* **59,** 169–185.

Mukougawa, H., and T. Ikeda, 1994: Optimal excitation of baroclinic waves in the Eady model. *J. Meteor. Soc. Japan,* **72,** 499–513.

Palmer, T. N., R. Gelaro, J. Barkmeijer, and R. Buizza, 1998: Singular vectors, metrics, and adaptive observations. *J. Atmos. Sci.,* **55,** 633–653.